# Twisted-nematic liquid-crystal-on-silicon adaptive optics aberrometer and wavefront corrector

**Seow-Hwang Eng**
Edith Cowan University
School of Engineering
270 Joondalup Drive
Joondalup, WA 6027
Australia

**Fred Reinholz**
Edith Cowan University
School of Engineering
270 Joondalup Drive
Joondalup, WA 6027
Australia
and
Lions Eye Institute
Lasers and Bioengineering Group
2 Verdun Street
Nedlands, WA 6009
Australia

**Douglas Chai**
Edith Cowan University
School of Engineering
270 Joondalup Drive
Joondalup, WA 6027
Australia

**Abstract.** A Hartmann-Shack wavefront sensor (HSWS) has been proven to be a reliable tool for the quantitative analysis of human ocular aberrations. In an active adaptive optics (AO) system, it has the role to monitor wave aberrations. To ensure the exclusive retrieval of Zernike coefficients for the measured ocular wavefronts, we first nullify the AO system's aberrations. This is of particular importance in our setup with a twisted-nematic (TN) liquid-crystal-on-silicon (LCoS) chip as the wavefront manipulator due to its strong unwanted zero-order diffractive beam. We characterize the AO system's performance—before and after ocular corrections—by means of different parameters, including experimental and simulated point spread functions (PSFs). An iterative closed-loop algorithm reduces the residual wavefront error to typical values of 0.1 $\mu$m. This system constitutes a wavefront corrector that can possibly be used for high resolution retinal imaging purposes or for visual psychophysical experiments. 
[DOI: 10.1117/1.3183814]

Keywords: aberrations; adaptive optics; spatial light modulator; liquid crystals; diffractive optics; vision.

Paper 09059R received Feb. 20, 2009; revised manuscript received May 27, 2009; accepted for publication May 27, 2009; published online Jul. 27, 2009.

## 1 Introduction

Retinal imaging is one of the most important tools in ophthalmology and vision science. Traditionally, flashlight-illuminated, film-based fundus cameras have been used in a variety of modes (such as red free, stereo, and angiography) for retinal photography. In recent times, digital cameras have replaced film cameras in many image recording devices, providing superior imaging performance without any major changes to the optical layout. On the other hand, novel retinal imaging technologies have been developed to significantly increase the quality of retinal images. Monochromatic scanning laser ophthalmoscopy (SLO) produces images of higher contrast due to reduced scattering from neighboring retinal structures. Confocal SLO—with its depth discrimination ability—allows for optical sectioning and the acquisition of 3-D retinal images.[1,2] Polarization-sensitive SLOs can analyze thicknesses of birefringent layers such as the nerve fiber layer, and multiple wavelength SLOs combine the advantages of color photography and scanning technology.[3] Optical coherence tomography (OCT) works at similar lateral resolutions as fundus cameras or SLOs, but owing to its interferometric measurement principle, a transversal resolution of single-digit microns can be achieved.[4]

Address all correspondence to: Seow-Hwang Eng, School of Engineering, Edith Cowan University, 270 Joondalup Drive, Joondalup WA6027, Australia; Tel.: +61863045318; Fax: +61863045493; E-mail: seowe@student.ece.edu.au

Due to the nature of the human eye, retinal imaging is a far-field optical technology governed by the laws of reflective microscopy. Applying Rayleigh's criterion:

$$\Delta_{LR} = 1.22 f\lambda/D,$$

gives the best lateral resolution $\Delta_{LR}$ for diffraction-limited imaging by using the shortest wavelength (in the order of $\lambda$ =400 nm) that is transmitted through the eye and the largest pupil diameter ($D$=8 mm). From these numbers—with an effective focal length $f$=16.6 mm in air—a lateral resolution of 1 $\mu$m is the theoretical limit. In practice, the shortest imaging wavelength is about 500 nm (to avoid phototoxicity), but for patient comfort, near-IR light ($\sim$700 nm) is often used. Furthermore, the normal human ocular system delivers a diffraction-limited performance only for beam diameters up to 3 mm. Therefore, with a standard retinal imager, the achievable resolution is limited to 3.5 to 5 $\mu$m. To achieve resolutions closer to the theoretical limit, wavefront distortions caused by ocular imperfections and biological variability have to be rectified. This can be realized with an active adaptive optics (AO) system that corrects ocular wavefronts. With a wavefront sensor and a wavefront manipulator being the most essential components, the preferred detector in AO systems for eyes is the Hartmann-Shack wavefront sensor (HSWS), while deformable mirrors (DMs) (membrane or segmented) are the favored wavefront manipulators. Numerous high-

1083-3668/2009/14(4)/044014/7/$25.00 © 2009 SPIE

resolution full-field and scanning retinal imagers based on HSWS and DMs have been constructed,[5–10] and high quality images of the cellular structures in the living retina have been reported.[11,12] The primary factors limiting the use of DMs in AO systems include their low spatial resolution, high cost, high power consumption, and bulkiness.

Liquid crystal spatial light modulator (LC-SLM) chips also have the capability to act as wavefront manipulators. Recent advancements include the development of liquid-crystal-on-silicon (LCoS) chips, which exhibit high spatial resolution (up to 2 megapixels), high fill factor (90 to 100%), high diffraction efficiency, high reflectivity, low cost, and fast switching times. While the primary use of these chips is in display technology, they can also be configured to act as optical switches,[13] diffractive optical elements,[14,15] polarization manipulators,[16] or phase shifters.[17,18] Due to their pixelated nature, inactive interpixel regions, and piston-only movements, SLMs will, in general, generate beams of multiple diffraction orders when impinged by a single oncoming beam. Depending on the properties of the oncoming beam and the settings of the SLM, properties such as direction, phase, polarization, and intensity of the departing beams can be modified. In most applications, only the first-order diffracted beam is required. However, systems that utilize multiple beams have also been reported.[19] Because there are limitations to which the properties of the zero-order beam can be altered, its presence can have negative impacts on an optical system's efficiency. The contribution of this unwanted beam is particularly strong in a twisted-nematic (TN) LCoS chip due to polarization direction mismatch.[20–22] On the other hand, TN-LCoS chips are more widely available at lower costs than their parallel aligned (PAL-LCoS) counterparts.

In a previous work, we investigated the use of a TN-LCoS-SLM in a setup for measurements and compensations of static aberrations in an artificial eye.[23] In this work, we provide adaptive optical corrections to human eyes by the application of the TN-LCoS-SLM and a HSWS. The AO setup offers complete ocular wavefront measurements and corrections. Our approach provides a study on the feasibility of using TN-LCoS-SLMs as wavefront correctors in retinal imaging systems.

## 2 Experimental

### 2.1 *Setup and Methods*

The schematic diagram of the system's double-pass optical layout is shown in Fig. 1. In the dynamic compensation experiments with human eyes, the illumination source is a 645-nm laser diode, which intensity can be adjusted by neutral density filters (NDFs). The off-axis aperture AP1 limits a beam diameter of 1.5 mm entering human eyes. This off-center illumination aids in the removal of bright corneal reflections to avoid corrupting the HSWS images. The input beam is reflected by a 5/95 R/T ratio wedge beamsplitter (WBS) toward the eye. The ocular optics focus this beacon beam to a point on the retina so that the beam reflected from this spot will be detected by the HSWS. Both the WBS and aperture stop AP4 prevent ghost reflections exiting the eye from entering the rest of the optical system. The wavefront corrector is a TN-LCoS-SLM (Holoeye LCR-2500) with XGA resolution, a 93% fill factor, and a phase modulation

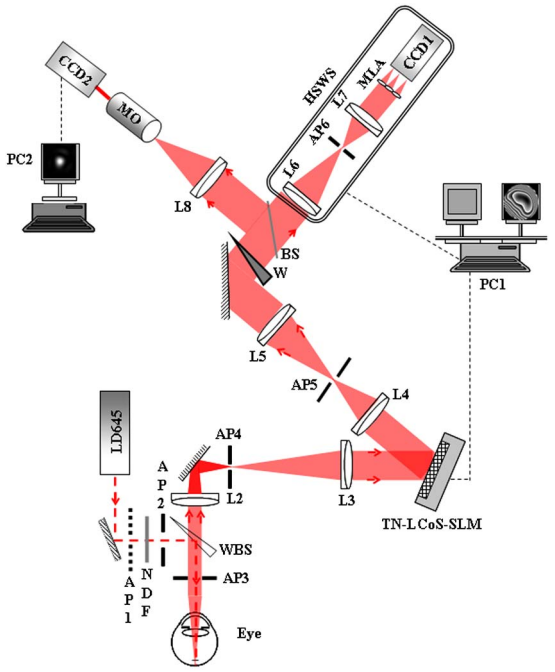


**Fig. 1** Schematic setup of system for AO wavefront correction with human eyes.

depth of $2\pi$. The phase modulation capability of this SLM has been studied and reported in Ref. 24. The addressing of the SLM is performed through phase-wrapped representations in bitmap format, and the device has been optimized to work with visible wavelengths. A telescopic system (consisting of lenses L2 and L3) is used to magnify the eye pupil plane by a factor of 2 onto the SLM plane. Beam separation at the SLM is achieved by a tilt of 5 deg.

As the SLM exhibits a strong zero-order contribution, an initial wavefront of $\varphi|_{PR}$ (a diffractive blazed grating of 11.8 lines/mm) is addressed onto the SLM to separate the different diffraction orders. Aperture AP5 allows only the propagation of the useful first-order beam to be sampled by the HSWS. To redirect this beam back onto the optical axis of the system, a 0.5 diopter ($D$) glass prism ($W$) is placed at the conjugate pupil plane.

The HSWS has a total of 812 active sampling microlenslets. It was custom-made by the Institute of Optics and Electronics, Chengdu, China. Each microlenslet has a pitch of 130 $\mu$m and a focal length of 4.8 mm. Incorporated in the HSWS is a telescopic system (lenses L6 and L7) that puts the conjugate pupil plane 200 mm in front and requires a maximum 20-mm-diam input beam. The telescope made up of lenses L4 and L5 provides the correct beam diameter, and a magnification of 1.5. CCD1 is a standard 1/3″ chip TV camera with a resolution of 640×480 pixels. The sampling of the complete wavefront is performed by averaging the wavefront's slope across each microlenslet's aperture, which is proportional to the displacement of the focused spots from their points of origin. A centroiding algorithm is employed to determine the position of each focused spot. Employing the modal wavefront reconstruction algorithm, the measured wavefront is decomposed into the first 65 Zernike coefficients

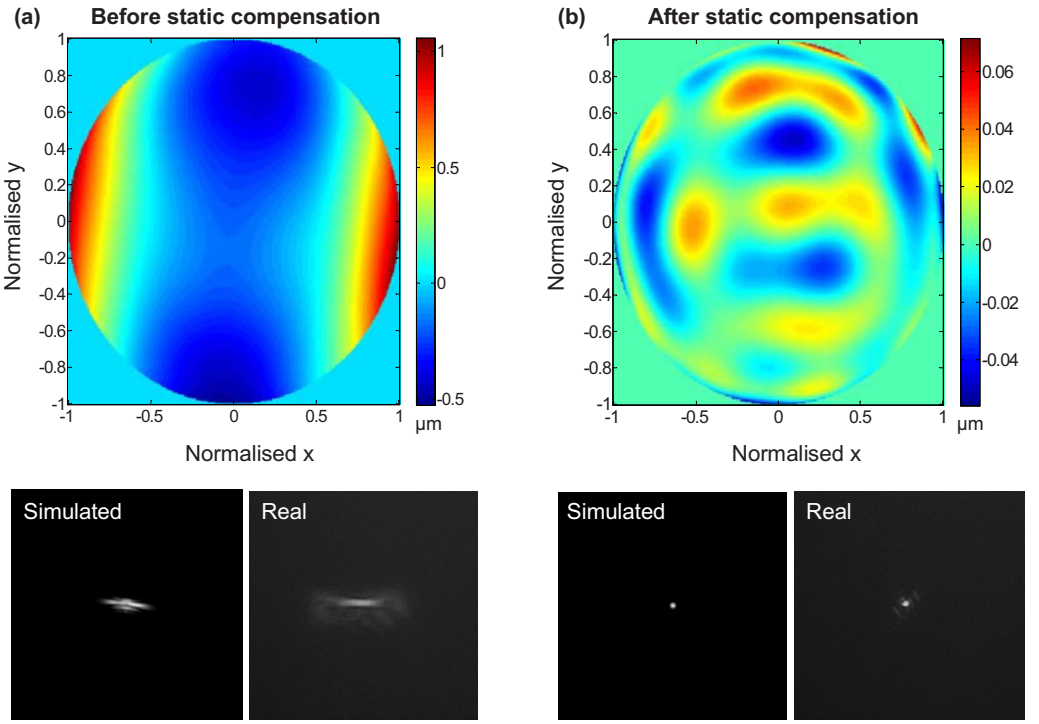


**Fig. 2** Wavefront measurements (units in $\mu$m) and PSFs of the system's inherent aberration (a) before and (b) after open-loop correction. Dimensions of each PSF image: 120×120 $\mu$m at retinal plane.

by our software. Our wavefront reconstruction software (implemented in MATLAB) facilitates for the analysis of wavefronts of different pupil diameters. Therefore, depending on the size of the pupils, the number of microlenslets to be considered for the centroiding algorithm is scaled accordingly. The control of the SLM's device driver, the readout of the HSWS, and the closed-loop algorithm (also implemented in MATLAB) are performed by computer PC1.

Lens L8 (f=100 mm) and a 20× microscope objective (MO) are used to image and magnify the PSF from the eye's retinal plane into a charge-coupled device (CCD) camera (CCD2: Pulnix TM-200), which is connected to computer PC2 to monitor the system's performance. The PSF of the eye under investigation viewed from this CCD camera has undergone a total magnification of 40×.

Inherent wavefront errors are present in the system due to 1. the imperfections of simple lenses used in the telescopes, 2. spatial misalignments of optical components, 3. tilted position of the SLM, and 4. potentially nonflat reflective backplane of the SLM. Comprising mainly of astigmatism and defocus, the collective result of these contributions is shown in Fig. 2(a), and their effects on the system's retinal plane are also illustrated. Both the experimentally obtained and simulated (computed from the HSWS' readings) PSFs show comparable features, illustrating the coherence of measurements in both pupil and retinal planes. To eliminate these static aberrations from the system, an artificial eye with a perfect reflector as retina is placed in the pupil plane (Fig. 1). An open-loop correction has been carried out to nullify these inherent aberrations, thus placing a corrective wavefront ( $\varphi|_{\text{inherent}}$) onto the SLM. The residual wavefront error in the system has been minimized to provide diffraction-limited imaging, as illustrated by the narrowed PSFs in Fig. 2(b). Subsequent measurements of the human eye are thus carried out with an initial corrective wavefront of ( $\varphi|_{PR}+\varphi|_{\text{inherent}}$) addressed onto the SLM. This approach of initially eliminating the system's inherent aberration enables the quantification of aberrations contributed by human eyes only.

### 2.2 *Correction of Ocular Aberrations*

The AO system was tested with four subjects without their vision aids on (for those who normally need them). During the experiments, the beam intensity is limited to 20 $\mu$W. The Human Research Ethics Committee at Edith Cowan University approved this study, and informed consent had been requested from all subjects prior to their participation. The pupil of each subject's left eye was dilated with a drop of 1% Tropicamide, and data collection did not commence until the pupil reached a minimum diameter of 6.5 mm. In the experiments, a rigid forehead-and-chin rest that can be readily translated in the *xyz*-directions is used to position the subject's head. After the correct position is found, the translators are locked. To ensure the eye's pupil stays centered with respect to the optical axis of the AO system, the raw images from the HSWS are observed. Performing this procedure achieves an adjustment accuracy and stability very similar to that of a commercial aberrometer. Studies have shown that small alignment errors in the order of ±2 mm are of little consequence for clinical wavefront measurements with a HSWS, as long as the pupil stays centered and bite bars are not needed.[25,26] Each subject is required to fixate on the incoming laser beacon, which was placed at infinity. The laser beacon is reflected off the subject's retina and guided out through the optics of the eye,

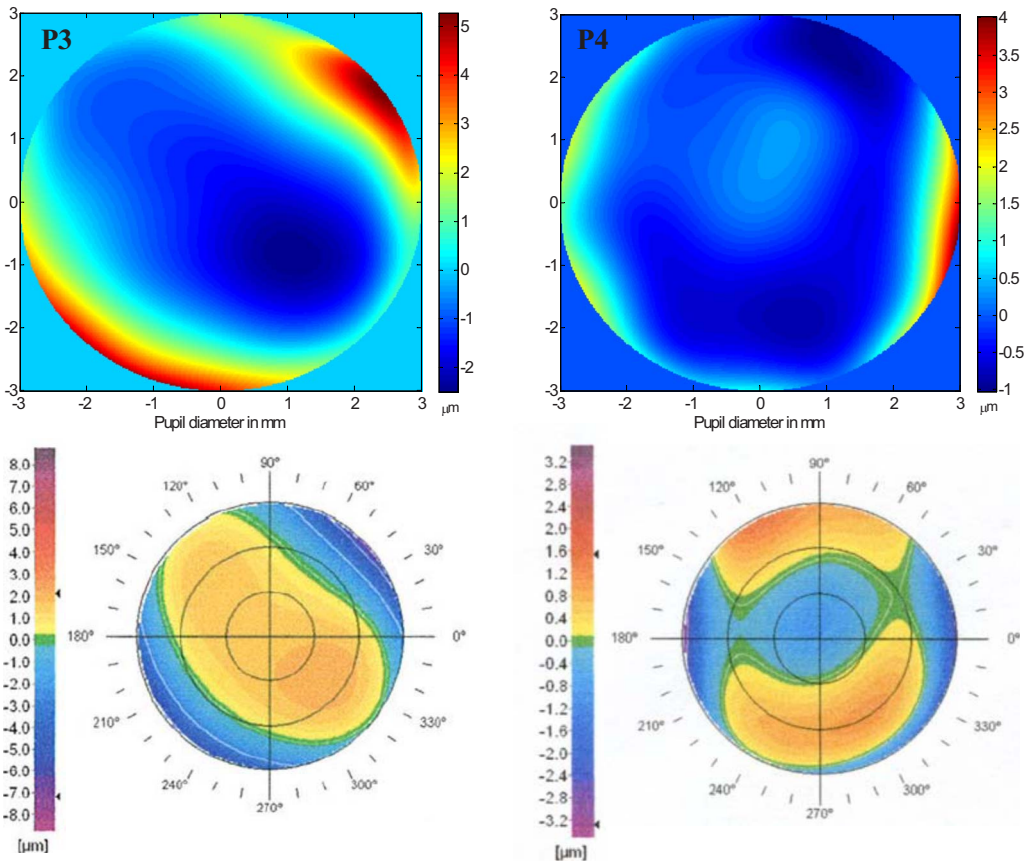


**Fig. 3** Ocular measurements of subjects P3 and P4 from the HSWS used in the setup with 5.9-mm dilated pupils (top) and a commercial Zywave aberrometer with 6-mm dilated pupils (bottom).

thereby sampling its aberrations. Head positions had to be adjusted repeatedly to align the subject's pupil with respect to the HSWS. Once the subject's eye position is stabilized, the subject is asked to maintain fixation on the beam while eye measurements were taken and the loop is closed. Both the SLM and the HSWS are positioned conjugated to the pupil plane of the subjects' eyes. Through the commencement of the closed-loop control algorithm, the SLM performs the compensation of the phase wavefronts of the eye aberrations from the readings of the HSWS. The correction was achieved over a pupil of 5.9 mm diam, corresponding to an area of 110 $mm^2$ on the SLM and 608 sampling points on the HSWS. The performance of the system during measurements and corrections can be observed through real-time viewing of: 1. the changes of the Zernike terms, ocular wavefront, and rms wavefront error (from an interface in PC1); and 2. the real-time experimental PSF (from PC2). To fully benefit from the high resolution of the SLM, the closed-loop algorithm incorporates a unity gain factor for the first corrective step and 0.3 for subsequent steps.

After writing the initial static corrective wavefronts to the SLM, the wavefronts of four subjects' left eyes (P1, P2, P3, and P4) are measured. With the approach of compensating for the static aberrations in the system first, the measurements of only the aberrated pupils can be obtained without data contamination. Subjects P3 and P4 have had their eyes measured by a Bausch and Lomb aberrometer (Zywave® II) at the Lions Eye Institute, Perth. The ocular measurements using the Zywave aberrometer were performed over the central 6 mm of the dilated pupils. Figure 3 shows the comparison of ocular measurements obtained from this aberrometer (bottom) and those from the HSWS in our system (top). Both reconstructions are in good agreement, both in shape and in the range of aberrations, supporting the validity of our method used.

Figure 4 shows the dynamic changes of ocular measurements for these four subjects over 60 sec. The first halves of the plots show the evolution of the wavefront rms of the eyes before the compensation process. The fluctuation of the rms wavefront error is contributed by ocular dynamic behavior, head or eye movements, and/or blinking. Before AO correction, the subjects' rms wavefront error ranged from 0.35 to 1.58 $\mu$m. The AO system is switched on after 45 consecutive eye measurements have been performed, the effects of which are indicated in the second halves of the plots in Fig. 4. On average, the system takes 2 sec for the SLM to fully produce the required conjugated wavefronts. Through the dynamic compensations of the eyes' aberrations, residual rms values ranging from 0.07 to 0.22 $\mu$m were achieved for the 5.9-mm dilated pupils. The wavefront in phase-wrapped representations before (averaged) and after (best-measured) correction are also illustrated for each subject in Fig. 4. The wavefronts after correction are most notably flatter for subjects P1 and P4.

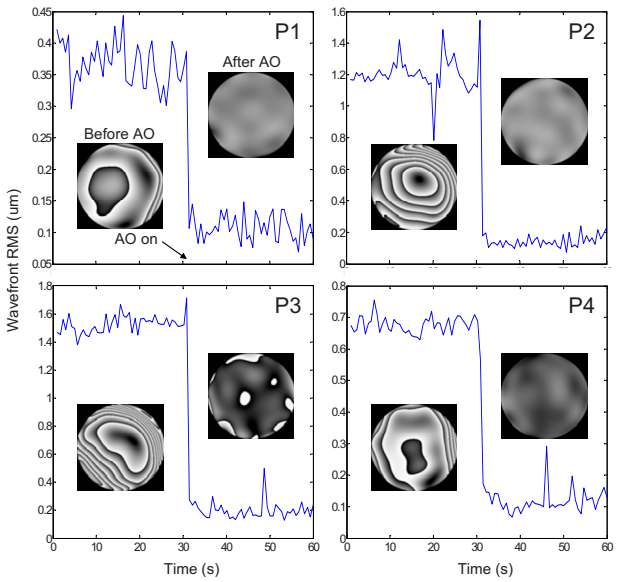


**Fig. 4** Temporal evolution of wavefront rms for subjects P1, P2, P3, and P4 for 5.9-mm pupils. AO is switched on after the first 30 sec of measurements. Inserted are corresponding ocular aberrations in phase-wrapped representations before and after correction.

The global performance of the system cannot be concluded from the wavefront data only (through figures of merit such as rms values). For a more complete evaluation of our system's performance, we compared the recorded images of the point source in the retina with those computed from the wavefront estimates as shown in Fig. 5. The Strehl ratios (SRs) are also included with the simulated PSFs. They are computed from the averaged rms readings of the HSWS, and in the case of after AO correction, from the best-corrected wavefront for each subject. A quantitative comparison between the real and simulated PSFs was not possible due to noise and retinal speckles. However, the experimentally obtained and simulated PSFs without AO do have reasonable resemblance. In particular, subject P3's astigmatism of −1.25 D results in a characteristic PSF that bears undeniable similarities between the real and simulated cases. Once the AO system is switched on, the PSFs were observed to be more compact when the loop converges. The best SR achieved with our system from these subjects is 0.69 (subject P1). While the simulated PSFs indicated that perfect retinal images are achievable, the real PSFs showed otherwise: retinal speckles are observed to surround the central lobe of the Airy disk, and the degree of speckles introduced varies from subject to subject. Notwithstanding this, in all real corrected PSFs, the diameter of the Airy disk subtends an angle ~6.5 arc-min. All images are viewed at $120 \times 120$ $\mu$m at the retinal plane of the eye.

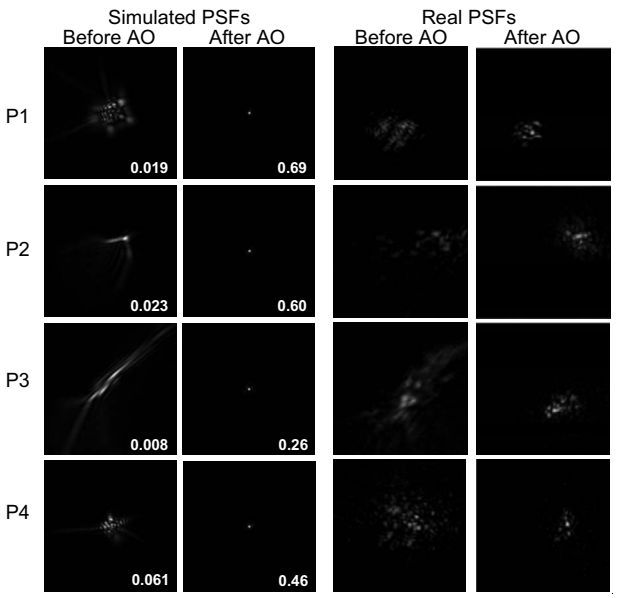


**Fig. 5** Comparison of experimentally obtained and simulated PSFs for four left eyes with and without AO correction. Calculated SRs are included in the simulated PSFs. The length of each image corresponds to 4.8 mm on CCD2 and 120 $\mu$m on the retina.

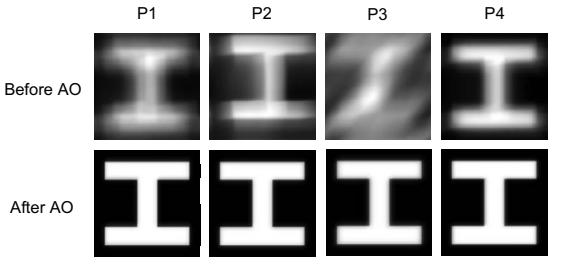


**Fig. 6** Estimated visual improvements after adaptive correction of ocular aberrations.

To provide an approximation to the subjects' visual acuity before and after dynamic ocular corrections, an optotype (symbol 𝕀) was convolved with the estimated PSF images, as shown in Fig. 6. The size of the 𝕀 symbol corresponds to the third row from the top of the Snellen chart, equivalent to 20/70 vision. In general, the subjects' visual performance is expected to have improved to 20/20 or even 20/16 after correcting their ocular aberrations. The image is particularly better resolved for subject P3, such that the optotype can easily be identified after AO correction.

## 3 Discussions and Conclusions

In the experiments conducted, we fully utilize the advantageous properties of the TN-LCoS-SLM, including its high resolution and the large stroke available as a result of phase wrapping. No trial lenses were therefore needed for any of the subjects tested. In addition to each subject's corrected ocular aberrations, the SLM's corrective wavefront also includes the static components necessary to separate the first-order beam from the zero-order contribution, and to compensate for the system's inherent aberrations. Reliable ocular measurements and corrections are therefore supported in this AO system. Assuming phase unwrapping, the final compensating wavefronts' peak-to-valley values are on the order of 100 $\mu$m. Such a large compensating span is made possible through the large number of pixels offered by the SLM. A wide dynamic range, however, comes at the expense of requiring an equally large bitmap pattern (phase-wrapped wavefront) to be calculated and uploaded onto the corrective device. This exhaustive computational effort would normally be expected to signifi-

cantly decrease the repetition rate of the setup. However, due to the slow-response time of the SLM, live reconstructions of the ocular wavefront that use a large number of correction modes can be accomplished without significant effects on the overall speed of the AO system. No additional delay was added to the loop to smooth the convergence of the system. The robustness of the closed-loop control method (allowing unity gain factor for first iteration) accomplishes the convergence of the SLM to the required wavefront in approximately three iterations giving a closed-loop bandwidth of 0.5 Hz. For comparison, most of the temporal fluctuations of the ocular aberrations for a paralyzed eye occur at frequencies lower than 2 Hz.[27] Beyond that, the eye's focus fluctuates about its mean level with frequencies up to 5 Hz,[28] and ocular aberrations at frequencies close to 30 Hz have also been detected.[29] We are currently using 608 microlenslets in the HSWS and computing 65 Zernike coefficients; reducing both these numbers to more appropriate figures may allow us to achieve a higher closed-loop bandwidth in conjunction with a faster SLM.

The simultaneous recording of PSFs during measurements and corrections has demonstrated the consistency of metrics in both the pupil (such as ocular wavefronts and Zernike decompositions) and retinal planes (i.e., Strehl ratios as well as both real and simulated PSFs), confirming the reliability and adequacy of the static compensation performed prior to the measurements of human eyes. No sampling, averaging, or delay occurs when obtaining the subjects' experimental PSFs. These PSFs bear some resemblance to those computed from the HSWS's readings. However, the quality of the experimental PSFs is compromised by speckles attributed by the long coherence length of the laser diode and a stationary beam used on the retinal surface. Although the use of superluminescent diodes at near-IR wavelengths may have eliminated most of the problem of retinal speckles in the PSFs, it was not implemented in the system, as the SLM is not optimized for wavelengths beyond the visible range. Furthermore, using the same light source for measurement, correction, and imaging will allow for full compatibility of all experimentally obtained and simulated data. On the other hand, this system—with a high-resolution HSWS—performs very precise aberration measurements. With more sophisticated techniques to accurately monitor or control the translational and angular positions, as well as the rotational state of the eye, it may be possible to correlate, for instance, the after-effects of blinking or gazing with the actual wavefront errors.

We achieve residual rms values of 0.1 to 0.2 $\mu$m, similar to those reported for most established AO systems for human eyes.[27,30,31] The SRs obtained after AO corrections vary from 0.26 to 0.69. A possible explanation for these relatively low SRs is that the speed of the convergence of the AO system (0.5 Hz) is too slow to adequately react to the dynamics of the eyes' optics. The system described here with a slow TN-LCoS-SLM can perform closed-loop corrections of eye aberrations in about 2 sec; it may therefore lack the agility to deal with rapid changes in the ocular dynamics. The computation of convolutions using the measured wavefront properties provides an estimation of the subjects' visual acuity before and after AO correction. It is anticipated that the wavefront corrections improves the subjects' visual performance to at least 20/20.

In summary, modeled on DM-based systems, this work of utilizing a TN-LCoS-SLM as the wavefront corrector is carried out to establish the suitability of such devices to be used in an AO retinal imaging system. So far, SLMs with parallel-aligned liquid crystals (PAL-SLMs) have been reported for the closed-loop correction of ocular aberrations in model[30,32] and human eyes,[30,33] in fundus imaging,[34] and in OCT retina cameras.[31] PAL-SLMs appear to be the more favorable option, for they are highly efficient phase-only modulators. For the same spatial resolution, TN-LCoS-SLMs are cost-effective alternatives. However, this particular type of SLM has limitations to its diffraction efficiency due to its strong zero-order beam. By allowing only the useful first-order diffracted beam to be used in the experiments, half the impinging beam's power is lost. This can have negative effects on the image quality (e.g., signal-to-noise ratio) achievable with an AO retinal imaging system based on TN-SLMs. The high optical losses may require the use of higher intensity light beams on the subjects' eyes or longer exposure times, potentially causing patient discomfort. Despite the TN-LCoS-SLM's presently achievable low closed-loop bandwidth and small operative wavelength band, the AO system can find applications in high resolution retinal cameras or can be used for visual psychophysical experiments.

## Acknowledgments

The authors would like to thank Kamal Alameh for the use of laboratory facilities at the Electron Science Research Institute.

## References

1. R. H. Webb, G. W. Hughes, and F. C. Delori, "Confocal scanning laser ophthalmoscope," *Appl. Opt.* **26**(8), 1492–1499 (1987).
2. R. O. W. Burk, K. Rohrschneider, H. E. Volcker, and G. Zinser, "Analysis of three-dimensional optic disc topography by laser scanning tomography," in *Scanning Laser Ophthalmoscopy and Tomography*, J. A. B. Nasemann and R. O. W. Burk, Eds., pp. 161–176, Quintessenz, Munich (1990).
3. F. Reinholz, R. A. Ashman, and R. H. Eikelboom, "Simultaneous three wavelength imaging with a scanning laser ophthalmoscope," *Cytometry* **37**(3), 165–170 (1999).
4. R. D. Ferguson and D. X. Hammer, "Tracking optical coherence tomography," *Opt. Lett.* **29**(18), 2139–2141 (2004).
5. A. Roorda, F. Romero-Borja, W. Donnelly III, H. Queener, T. Hebert, and M. Campbell, "Adaptive optics scanning laser ophthalmoscopy," *Opt. Express* **10**(9), 405–412 (2002).
6. Y. Zhang, S. Poonja, and A. Roorda, "MEMS-based adaptive optics scanning laser ophthalmoscopy," *Opt. Lett.* **31**(9), 1268–1270 (2006).
7. D. C. Chen, S. M. Jones, D. A. Silva, and S. S. Olivier, "High-resolution adaptive optics scanning laser ophthalmoscope with dual deformable mirrors," *J. Opt. Soc. Am. A* **24**(5), 1305–1312 (2007).
8. B. Hermann, E. J. Fernandez, A. Unterhuber, H. Sattmann, A. F. Fercher, W. Drexler, P. M. Prieto, and P. Artal, "Adaptive optics ultrahigh-resolution optical coherence tomography," *Opt. Lett.* **29**(18), 2142–2144 (2004).
9. G. Shi, Y. Dai, L. Wang, Z. Ding, X. Rao, and Y. Zhang, "Adaptive optics optical coherence tomography for retinal imaging," *Chin. Opt. Lett.* **6**(6), 424–425 (2008).
10. Y. Zhang, B. Cense, J. Rha, R. S. Jonnal, W. Gao, R. J. Zawadzki, J. S. Werner, S. Jones, S. Olivier, and D. T. Miller, "High-speed volumetric imaging of cone photoreceptors with adaptive optics spectral-domain optical coherence tomography," *Opt. Express* **14**(10), 4380–4394 (2006).
11. A. Roorda and D. R. Williams, "The arrangement of the three cone classes in the living human eye," *Nature (London)* **397**(6719), 520–522 (1997).

12. D. C. Gray, W. Merigan, J. I. Wolfing, B. P. Gee, J. Porter, A. Dubra, T. H. Twietmeyer, K. Ahmad, R. Tumbar, F. Reinholz, and D. R. Williams, "In vivo fluorescence imaging of primate retinal ganglion cells and retinal pigment epithelial cells," *Opt. Express* **14**(16), 7144–7158 (2006).
13. M. Aljada, S. Eng, and K. Alameh, "Design of 10 Gbps optical encoder/decoder structure for FE-OCDMA system using SOA and opto-VLSI processors," *Opt. Express* **16**(2), 679–685 (2008).
14. L. Zhao, N. Bai, X. Li, L. S. Ong, Z. P. Fand, and A. K. Asundi, "Efficient implementation of a spatial light modulator as a diffractive optical microlens array in a digital Shack-Hartmann wavefront sensor," *Appl. Opt.* **45**(1), 90–94 (2006).
15. C. Kohler, X. Schwab, and W. Osten, "Optimally tuned spatial light modulators for digital holography," *Appl. Opt.* **45**(5), 960–967 (2006).
16. F. Stabo-Eeg, K. Gastinger, O. Hunderi, and M. Lindgren, "Determination of the phase and polarization changing properties of reflective spatial light moulators in one set-up," *Proc. SPIE* **5618**, 174–182 (2004).
17. G. D. Love, "Wave-front correction and production of Zernike modes with a liquid-crystal spatial light modulator," *Appl. Opt.* **36**(7), 1517–1520 (1997).
18. L. Hu, L. Xuan, Y. Liu, Z. Cao, D. Li, and Q. Mu, "Phase-only liquid crystal spatial light modulator for wavefront correction with high precision," *Opt. Express* **12**(26), 6403–6409 (2004).
19. Z. Wang, R. Zheng, K. E. Alameh, R. Robertson, U. Muller, and L. Bloom, "Opto-VLSI based dynamic optical splitter," *Electron. Lett.* **40**(22), 1445–1446 (2004).
20. E. G. van Putten, I. M. Vellekoop, and A. P. Mosk, "Spatial amplitude and phase modulation using commercial twisted nematic LCDs," *Appl. Opt.* **47**(12), 2076–2081 (2008).
21. A. Hermerschmidt, S. Osten, S. Kruger, and T. Blumel, "Wave front generation using a phase-only modulating liquid-crystal based microdisplay with HDTV resolution," *Proc. SPIE* **6584**, 65840E (2007).
22. Z. Cao, Q. Mu, G. Dovillaires, T. Grandin, E. Lavergne, L. Hu, and L. Xuan, "Effect of the twisted alignment on the liquid crystal wavefront corrector," *Liq. Cryst.* **34**(10), 1227–1232 (2008).
23. D. Cai, S. Eng, N. Ling, and W. Jiang, "Using reflective LCoS display panel to compensate human eye aberrations," *Chinese J. Optoelectron. Laser* **19**(7), 992–995 (2008).
24. S. H. Eng, D. M. Cai, Z. Wang, K. Alameh, and W. H. Jiang, "Optimization of Liquid-Crystal Spatial Light Modulator for Precise Phase Generation," in *Conf. Optoelectron. Microelectron. Mat. Devices*, pp. 105–108 (2006).
25. X. Cheng, N. L. Himebaugh, P. S. Kollbaum, L. N. Thibos, and A. Bradley, "Test-retest reliability of clinical Shack-Hartmann measurements," *Invest. Ophthalmol. Visual Sci.* **45**(1), 351–360 (2004).
26. R. A. Applegate, C. S. Ballentine, and A. Roorda, "Is a bite-bar needed for Hartmann-Shack (H/S) wavefront sensing," *Invest. Ophthalmol. Visual Sci.* **42**(4), S604 (2001).
27. H. Hofer, P. Artal, B. Singer, J. L. Aragon, and D. R. Williams, "Dynamics of the eye's aberrations," *J. Opt. Soc. Am. A* **18**(3), 497–506 (2001).
28. W. N. Charman and G. Heron, "Fluctuations in accommodation: a review," *Ophthalmic Physiol. Opt.* **8**, 153–163 (1988).
29. L. Diaz-Santana, C. Torti, I. Munro, P. Gasson, and C. Dainty, "Benefit of higher closed-loop bandwidth in ocular adaptive optics," *Opt. Express* **11**(20), 2597–2605 (2003).
30. A. A. S. Awwal, B. J. Baumann, D. T. Gavel et al. "Characterization and operation of a liquid crystal adaptive optics phoropter," *Proc. SPIE* **5169**, 104–122 (2003).
31. E. J. Fernandez, B. Povazay, B. Hermann, A. Unterhuber, H. Sattmann, P. M. Prieto, R. Leitgeb, P. Ahnelt, P. Artal, and W. Drexler, "Three-dimensional adaptive optics ultrahigh-resolution optical coherence tomography using liquid crystal spatial light modulator," *Vision Res.* **45**(28), 3432–3444 (2005).
32. T. Shirai, "Liquid-crystal adaptive optics based on feedback interferometry for high-resolution retinal imaging," *Appl. Opt.* **41**(19), 4013–4023 (2002).
33. P. M. Prieto, E. J. Fernandez, S. Manzanera, and P. Artal, "Adaptive optics with a programmable phase modulator: applications in the human eye," *Opt. Express* **12**(17), 4059–4071 (2004).
34. T. Yamaguchi, N. Nakazawa, K. Bessho, Y. Kitaguchi, N. Maeda, T. Fujikado, and T. Mihashi, "Adaptive optics fundus camera using a liquid crystal phase modulator," *Opt. Rev.* **15**(3), 173–180 (2008).